Proc. 15th Int. Symp. Origin of Matter and Evolution of Galaxies (OMEG15)
JPS Conf. Proc. **31**, 011046 (2020)
https://doi.org/10.7566/JPSCP.31.011046

The S_{E1}-factor of Radiative α Capture on ^{12}C in the Cluster Effective Field Theory

Shung-Ichi Ando

School of Mechanical and ICT convergence engineering, Sunmoon University, Asan, Chungnam 31460, Republic of Korea

E-mail: sando@sunmoon.ac.kr

(Received August 30, 2019)

We review our recent study for an estimate of the S_{E1} factor of radiative α capture on ^{12}C at the Gamow-peak energy, E_G = 0.3 MeV, in the cluster effective field theory.

KEYWORDS: S_{E1}-factor, radiative alpha capture on carbon-12, effective field theory

1. Introduction

In the late 1970s, a phenomenological Lagrangian method is suggested by Weinberg [1] as an alternative of current algebra to calculate a hadronic matrix element at low energies, which exhibits the chiral $SU(2)\times SU(2)$ symmetry and the explicit symmetry breaking patterns. Skillful techniques are required for calculations of the current algebra to derive a hadronic amplitude, e.g., the electro pion production on a nucleon, considering CVC and PCAC and satisfying the results from the low energy theorem and the relations among vertex functions required by Ward-Takahashi identities [2,3]. Those results, including the radiative and non-radiative vector and axial-vector matrix elements of nucleon, nonetheless, are systematically and straightforwardly calculated from the chiral Lagrangian which embodies the symmetry requirement in heavy-baryon chiral perturbation theory [4–6]. The idea of the method has been developed in various ways, and the framework of those methods are now known as effective field theories (EFTs). For recent reviews of EFTs, see, e.g., Refs. [7, 8].

For a phenomenological study of a reaction by employing an EFT, one may expect the specifications listed below from an EFT: (1) It is a model-independent approach. (2) One needs to introduce a momentum scale to separate relevant degrees of freedom at low energies from irrelevant degrees of freedom at high energies. (3) The theory provides us a perturbative expansion scheme around a specified theoretical limit; counting rules, in powers of Q/Λ_H where Q denotes a typical momentum scale of a reaction and Λ_H does a high momentum scale, will be available. By using the counting rules, one can expand the amplitude order by order. (4) Coefficients appearing an effective Lagrangian may not be constrained by a mother theory but can be fitted to experimental data.

One might regard the construction of an EFT for a nuclear reaction as formidable because a nucleus is a many-body system, and its detailed structure is not easily described from the first principle. At low energies, that is, a long wavelength limit for an external probe, an amplitude constructed from an effective Lagrangian, which is represented in terms of relevant low energy degrees of freedom and embodies symmetry requirements, exhibits a specific expression at low energy limit and may well describe a response (or pole structures) by an external probe. As discussed above, a construction of an EFT for a nuclear reaction may be possible; the most important condition is (2) a clear separation scale while (4) the availability of experimental data for a reaction is also important to fix coefficients appearing in an effective Lagrangian. In the following, we review our study of the $E1$ transition of the radiative α capture on ^{12}C by constructing an EFT [9].

2. EFT for the ^{12}C(α,γ)^{16}O process

In the study of the radiative capture process, ^{12}C(α,γ)^{16}O, at the Gamow-peak energy E_G = 0.3 MeV employing an EFT, one may regard the ground states of α and ^{12}C as point-like particles whereas the first excited states of α and ^{12}C are chosen as irrelevant degrees of freedom, from which a large scale of the theory is determined [10]. Thus the expansion parameter of the theory is $Q/\Lambda_H \sim 1/3$ where Q denotes a typical momentum scale $Q \sim k_G$; k_G is the Gamow peak momentum, $k_G = \sqrt{2\mu E_G} \simeq 41$ MeV, where μ is the reduced mass of α and ^{12}C. Λ_H denotes a large momentum scale $\Lambda_H \simeq \sqrt{2\mu_4 E_{(4)}}$ or $\sqrt{2\mu_{12}E_{(12)}} \sim 150$ MeV where μ_4 is the reduced mass of one and three-nucleon system and μ_{12} is that of four and eight-nucleon system. $E_{(4)}$ and $E_{(12)}$ are the first excited energies of α and ^{12}C, respectively. Now one has a typical length scale at k_G as $k_G^{-1} \sim 5$ fm. Moreover, a length scale of the outgoing photon is $k'^{-1} \sim 20$ fm because the emitted photon energy is $E'_\gamma \sim 10$ MeV. Thus, the photon is not sensitive to the detailed structures of the nuclei, and the point-like nuclei may be reliable for the present study.

An effective Lagrangian for the radiative capture reaction up to next-to-leading order (NLO) is constructed in Eq. (1) in Ref. [9]. Thus, the radiative capture amplitude is systematically calculated by using propagators and vertex functions extracted from the Lagrangian. In Fig. 1, diagrams for dressed composite propagators of ^{16}O consisting of α and ^{12}C for $l = 1$ are depicted, in which the Coulomb interaction between α and ^{12}C is taken into account [10–12]. (An effect of the ground 0_1^+ state of ^{16}O to the elastic α-^{12}C scattering for $l = 0$ is studied in an EFT in Ref. [13].) In Fig. 2, diagrams of the radiative capture process from the initial $l = 1$ state to the ^{16}O ground (0_1^+) state are depicted, in which the Coulomb interaction between α and ^{12}C is taken into account as well.

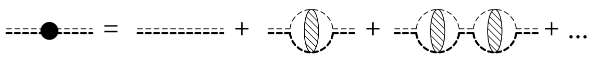

Fig. 1. Diagrams for dressed ^{16}O propagators. A thick (thin) dashed line represents a propagator of ^{12}C (α), and a thick and thin double dashed line with and without a filled circle represents a dressed and bare ^{16}O propagator, respectively. A shaded oval represents a set of diagrams consisting of all possible one-potential-photon-exchange diagrams up to infinite order and no potential-photon-exchange one.

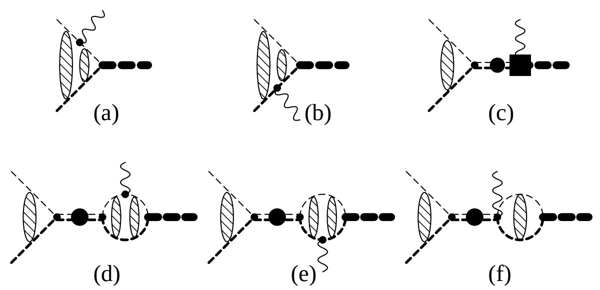

Fig. 2. Diagrams for the radiative capture process from the initial p-wave α-^{12}C state. A wavy line denotes the outgoing photon, a thick and thin double dashed line with a filled circle in the intermediate state, whose diagrams are displayed in Fig. 1, the dressed composite ^{16}O propagator for $l = 1$, and a thick dashed line in the final state the ground (0_1^+) state of ^{16}O. See the caption of Fig. 1 as well.

The radiative capture amplitude for the initial $l = 1$ state is presented as $A^{(l=1)} = \vec{\epsilon}^{\,*}_{(\gamma)} \cdot \hat{p} X^{(l=1)}$, where $\vec{\epsilon}^{\,*}_{(\gamma)}$ is the polarization vector of outgoing photon and $\hat{p} = \vec{p}/|\vec{p}|$; $\vec{p}$ is the relative momentum of the initial α and ^{12}C. The amplitude $X^{(l=1)}$ can be decomposed as

$$X^{(l=1)} = X^{(l=1)}_{(a+b)} + X^{(l=1)}_{(c)} + X^{(l=1)}_{(d+e)} + X^{(l=1)}_{(f)}, \quad (1)$$

where those amplitudes correspond to the diagrams depicted in Fig. 2. We follow the calculation method suggested by Ryberg *et al.* [14], in which Coulomb Green's functions are represented in the coordinate space satisfying appropriate boundary conditions. Thus we obtain the expression of those amplitudes in Eqs. (5), (6), (7), and (8) in Ref. [9].

3. Numerical results and discussion

We have five parameters to fix remained in the radiative capture amplitudes in Eq. (1). The three effective range parameters r_1, P_1, and Q_1 are fitted to the phase shift data for $l = 1$ from Tischhauser *et al.*'s paper [15]. Thus we have $r_1 = 0.415272(9)$ fm^{-1}, $P_1 = -0.57473(9)$ fm, $Q_1 = 0.02018(3)$ fm^3, where we have used the data in the α energy range, $2.6 \le E_\alpha \le 6$ MeV; the number of the data is $N = 273$, and $\chi^2/N = 0.74$. In the left panel of Fig. 3, we plot a curve of the phase shift δ_1 as a function of the α energy by using the fitted values of the parameters with the experimental data. One can see that our result well reproduce the experimental data.

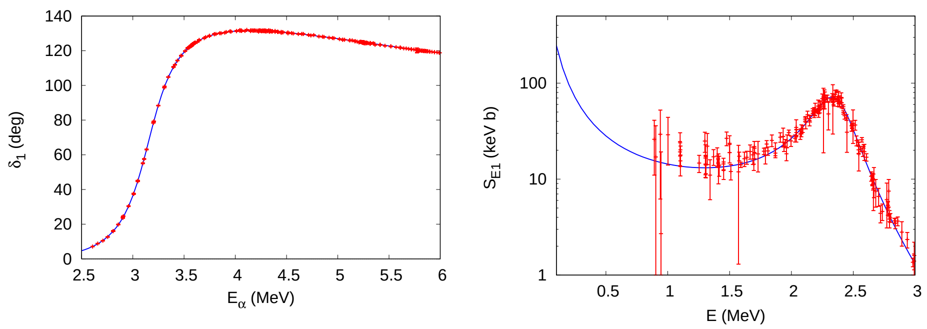

Fig. 3. (Left panel) Phase shift, δ_1, plotted by using the fitted effective range parameters, r_1, P_1, Q_1 as a function of E_α. The experimental phase shift data are also displayed in the figure. (Right panel) S_{E1} factor plotted by using the fitted parameters with $r_C = 0.1$ fm as a function of E. The experimental data are also displayed in the figure.

The remaining two parameters $h^{(1)R}$ and $y^{(0)}$ are fitted to the experimental data of the S_{E1}-factor in the energy range, $0.9 \le E \le 3$ MeV, where E is the initial energy of α-^{12}C system in the CM frame. The experimental data of the S_{E1}-factor are well summarized in Tables V and VII in Ref. [16]. In Table 1 in Ref. [9], we display the fitted values of $h^{(1)R}$ and $y^{(0)}$, χ^2/N, and S_{E1} at E_G as functions of the cutoff r_C where N is the number of the data, $N = 151$. The cutoff r_C is introduced because the loops in the diagrams (d) and (e) in Fig. 2 exhibit a log divergence at the $r \to 0$ limit, and the log divergence is renormalized by the coupling constant $h^{(1)R}$. One can see in the table that the significant cutoff dependence in $h^{(1)R}$ and $y^{(0)}$, and χ^2/N become larger and S_{E1} does smaller as r_C increases. In our work, we choose the results of S_{E1} for $\chi^2/N \le 1.7$ as our result. Thus we estimate a value of the S_{E1}-factor at E_G as $S_{E1} = 59 \pm 3$ keV b. In the right panel in Fig. 3, we plot a curve of S_{E1}-factor as a function of E for the cutoff $r_C = 0.1$ fm including the experimental data. One can see that the theory curve well reproduces the data. The previous estimates of the S_{E1} factor at E_G are well summarized in Table IV in Ref. [16]. The reported values are scattered from 1 to 340 keV·b with various size of the error bars. Nonetheless, it is worth pointing out that our result is about 30% smaller than those reported recently, e.g., $S_{E1} = 86.3$ keV b reported by deBoer *et al.* (2017) [16].

Lastly, we discuss a strong suppression mechanism of the $E1$ transition, which appears between isospin-zero ($N = Z$) nuclei. This mechanism is recently reviewed and studied for $\alpha(d,\gamma)^6$Li reaction by Baye and Tursunov [17]. In the standard microscopic calculations with the long-wavelength approximation, the term proportional to $Z_1/m_1 - Z_2/m_2$ vanishes because of the standard choice of the mass of nuclei as $m_i = A_i m_N$ where A_i is the mass number of the i-th nucleus and m_N is the nucleon mass. We have strongly suppressed but non-zero contribution because of the use of the physical masses for α and ^{12}C. The small but non-vanishing $E1$ transition for the $N = Z$ cases has intensively been studied in the microscopic calculations and can be accounted by two effects: one is the second-order term of the $E1$ multipole operator in the long-wavelength approximation [18], and the other is due to the mixture of the small $T = 1$ configuration in the actual nuclei [19]. In the present approach, the first one may be difficult to incorporate for the point-like particles while the second one could be introduced from a contribution at high energy: At $E \simeq 5$ MeV and 8.5 MeV above the α-^{12}C breakup threshold, p-^{15}N and n-^{15}O breakup channels, respectively, are open, and $T = 1$ resonant states of ^{16}O start emerging (along with the $T = 1$ isobars, ^{16}N, ^{16}O, and ^{16}F). We might have introduced the p-^{15}N and n-^{15}O fields as relevant degrees of freedom in the theory. The p-^{15}N and n-^{15}O fields, then, appear in the intermediate states, as p-^{15}N or n-^{15}O propagation, in the loop diagrams (d), (e), (f) in Fig. 2 instead of the α-^{12}C propagation. One may introduce a mixture of the isospin $T = 0$ and $T = 1$ states in the p-^{15}N or n-^{15}O propagation, and the strong $E1$ suppression is circumvented in the loops. (The contribution from the p-^{15}N and n-^{15}O channels for the ^{12}C(α,γ)^{16}O reaction has already been studied in the microscopic approach [20].) In the present work, however, the p-^{14}N and n-^{15}O fields are regarded as irrelevant degrees of freedom at the high energy and integrated out of the effective Lagrangian. Its effect, thus, is embedded in the coefficient of the contact interaction, the $h^{(1)R}$ term, in the (c) diagram while the $h^{(1)R}$ term is fitted to the experimental S_{E1} data. Inclusion of the p-^{15}N and n-^{15}O open channels in an EFT would be important for a quantitative study of the $E1$ suppression mechanism.

This work was supported by the National Research Foundation of Korea (2016R1D1A1B03930122 and 2019R1F1A1040362).

References

[1] S. Weinberg, Physica A **96**, 327 (1979).
[2] K. Ohta, Phys. Rev. C **46**, 2519 (1992).
[3] K. Ohta, Phys. Rev. C **47**, 2344 (1993).
[4] V. Bernard, N. Kaiser, T. S. H. Lee, and U.-G. Meißner, Phys. Rep. **246**, 315 (1994).
[5] S. Ando and D.-P. Min, Phys. Lett. B **417**, 177 (1998).
[6] S. Ando, F. Myhrer, and K. Kubodera, Phys. Rev. C **63**, 015203 (2001).
[7] H.-W. Hammer, C. Ji, and D.R. Phillips, J. Phys. G **44**, 103002 (2017).
[8] H.-W. Hammer, S. Konig, and U. van Kolck, arXiv:1906.12122 [nucl-th].
[9] S.-I. Ando, Phys. Rev. C **100**, 015807 (2019).
[10] S.-I. Ando, Eur. Phys. J. A **52**, 130 (2016).
[11] S.-I. Ando, Phys. Rev. C **97**, 014604 (2018).
[12] H.-E. Yoon and S.-I. Ando, J. Korean Phys. Soci. **75**, 202 (2019).
[13] S.-I. Ando, J. Korean Phys. Soci. **73**, 1452 (2018).
[14] E. Ryberg, C. Forssén, H.-W. Hammer, and L. Platter, Phys. Rev. C **89**, 014325 (2014).
[15] P. Tischhauser *et al.*, Phys. Rev. C **79**, 055803 (2009).
[16] R. J. deBoer *et al.*, Rev. Mod. Phys. **89**, 035007 (2017), and references therein.
[17] D. Baye and E. M. Tursunov, J. Phys. G: Nucl. Part. Phys. **45**, 085102 (2018).
[18] P. Descouvemont and D. Baye, Phys. Lett. B **127**, 286 (1983).
[19] P. Descouvemont and D. Baye, Nucl. Phys. A **459**, 374 (1986).
[20] P. Descouvemont and D. Baye, Phys. Rev. C **36**, 1249 (1987).